Long Term Project Report : Interim/Final

Summary Page

Proposal Number: MI-1355

1. Beamtime Used

Please give a short summary of progress for each scheduling period for which beamtime has been allocated/used :

Scheduling period	Beamline(s) Used	Shifts Used	Summary of results obtained
2020/II	none	0	no beamtime due to the COVID-19 pandemic restrictions.
2021/I	ID13	12	29.06.-01.07. Dresden Group: 1st installation of MLLs (multilayer Laue lenses) after the ESRF-EBS upgrade including a characterization with different prefocusing setups, mainly high-resolution setups with ~ nm FWHM focus size. One MLL stayed at ID13 for other users/beamtimes. Leoben Group: Due to travel restrictions, only remote experiment was performed, namely cross-sectional characterization of hard Coatings from Leoben using the new optics.
2021/II	ID13	12	09.09.-11-09. Dresden Group: Installation and characterization of a MLL with long working distance and ~ 80 nm FWHM focus size. MLL stayed at ID13 for other users/beamtimes. Leoben Group: Optimization and integration of the indenter system for ID13 and in-situ indentation of micro-cantilevers machined from nanocrystalline FeCr alloys. Cross-sectional characterization of nitride and diamond hard coatings and laser-diced silicon chips using the new optics at ID13. Transfer of the newly-developed indentation system to ID13 – the system can be now used by all users.
2022/I	ID13	12	18.-24.1.2022 Dresden Group: Characterization of several prepared single MLLs by tilt series and PCO camera images First test of the new MLL lens holder with improved internal alignment capabilities

			Assembly, alignment and characterization of a new MLL with long working distance. Stayed at ID13 for other users/beamtimes. <u>Leoben Group:</u> Further optimization and integration of the indenter system for ID13. In-situ indentation studies on nanocrystalline metals were performed. Additionally, mapping of microstructure and strain in MOSFETs and diamond coatings was performed
2022/II	ID13	12	24.-30.5.2022 <u>Dresden Group:</u> Characterization of the still installed MLL from January. Characterization of several prepared single MLLs by tilt series and PCO camera images. Attempt to align a new high resolution MLL. Re-Installation of the existing MLL with long working distance. <u>Leoben Group:</u> A new in-situ setup was developed for ID13 to follow growth of Li dendrites across solid state LLZO electrolytes during Li-ion battery cycling. The setup was successfully used to monitor the dendrite morphology evolution. Additionally, scanning experiments on microelectronic structures and hard coatings were performed. 06.-08.09.2022 <u>Dresden Group:</u> Characterization of the still installed MLL from May. Characterization of further MLLs, acquiring of test data for ptychographic characterization; diffraction efficiency measurements. Re-Installation of the existing MLL with long working distance.
2023/I			
2023/II			

2. Resources Provided by User team (financial, personnel, technical...):

<u>Dresden Group:</u> the experiments in January, May and September 2022 were performed by two or three scientists, Mr. Peter Gawlitza, Dr. Saeed Mizaei and Dr. Sven Niese (in general on-site, one times partially remote).
After each MI-1355 beamtime the best performing long-distance MLL from January 2022 was left at ESRF for other users/experiments.
Approximate prices for such MLLs are ~ 50 k€ (high-resolution MLL) and ~ 80 k€ (long-distance MLL).
<u>Leoben Group:</u> the experiment in June was performed remotely.

In September 2021, the in-situ and static experiments were performed by three scientist, Dr. Juraj Todt, Dr. Michael Meindlhumer and Mr. Tobias Ziegelwanger. An indentation system with the software developed in Leoben was handed over to ESRF and can be now used by the bright user community. Approximate price is ~40k€.

In January 2022, the experiment was performed by 4 users from Leoben. The indentation system developed for ID13 was further optimized in order to make it more user-friendly.

In June 2022, the experiment was performed by 2 users. A new dedicated operando setup for tracking of Li dendrite growth in solid-state Li-ion batteries was tested at the ID13. The long-term aim is to finalize the setup and leave at the beamline after the LTP finish, similar as it was done with the indenter.

3. **Technical and Scientific Milestones Achieved** (in relation to the milestones identified in the original proposal)**:**

Year 1

> In accordance with the proposed milestones, following results/milestones were achieved:

- First nanodiffraction experiments with improved crossed setup for long and short MLLs (compared to MI-1216) were performed (Figs. 1 and 2).
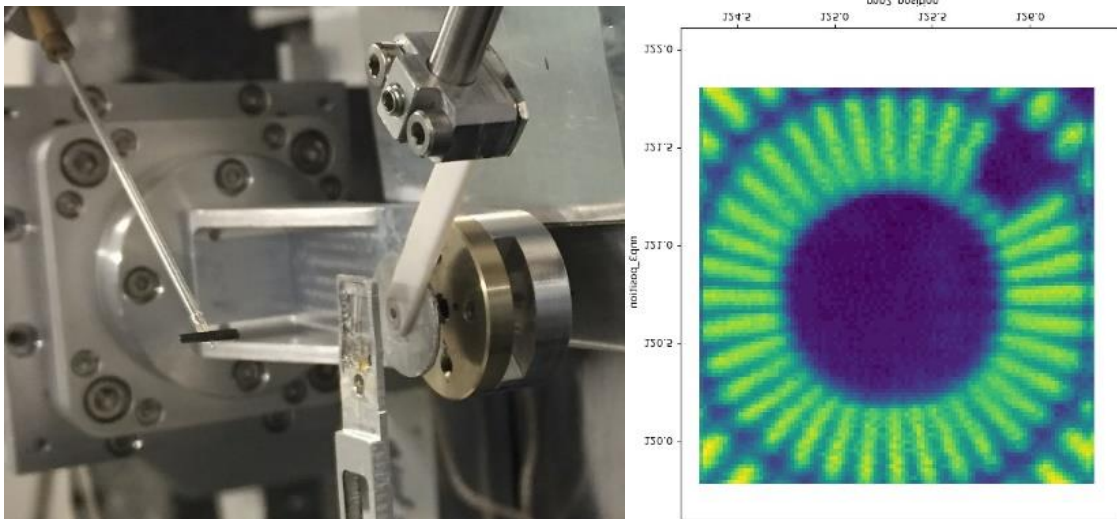

Fig.1: ID13 setup with a **high-resolution MLL optics**, order-separating aperture (OSA) and test sample in the focal plane, approx. 10 mm behind the optics @13 keV (left). Right: 2x2 µm² transmission scan of the Siemens star pattern in the focal plane of the MLL: the innermost 50 nm structures can be clearly resolved (beamtime 2021/I).
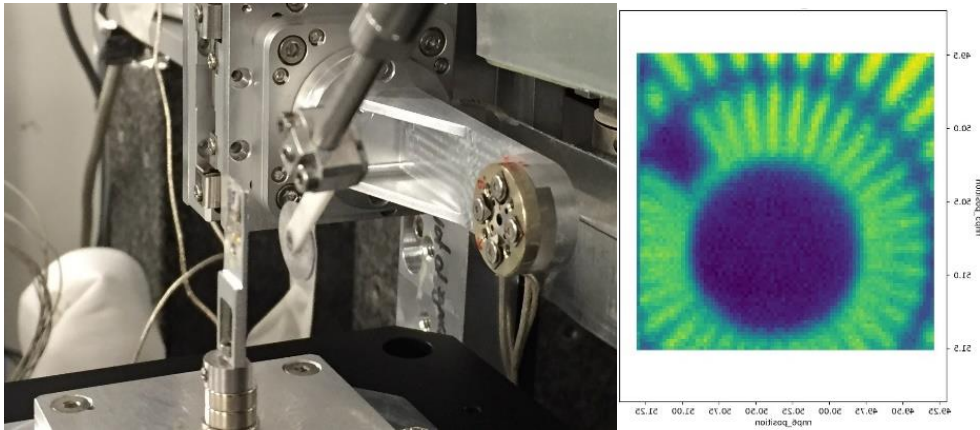
Fig.2: ID13 setup with **long-distance MLL optics**, OSA and test sample in the focal plane, approx. 50 mm behind the optics @13 keV (left). Right: 2x2 µm² transmission scan of the Siemens star pattern in the focal plane of the MLL: the 100 nm structures can be clearly resolved (beamtime 2021/II).

- Test of crossed MLLs with a large working distance and a fully usable aperture of 100 µm was performed.
- Improved flux (compared to last beamtime before ESRF-EBS upgrade) of more than 4e+20 photons/mm² Si(111)-monochromatic flux density @13 keV (>2 orders of magnitude more than the current ID13 record) was recorded.
- Ptychographic reconstruction of the diffracted beam of the long-distance MLL setup showed a focal size of **approx. 80x80 nm²** and a focal depth of about 50 µm. Diffraction efficiency measurements of this MLL @13keV with 100x100 µm² aperture resulted in a photon ratio of approx. 44% into the first order focused beam.
- MLLs with long and short working distances were left at ID13 for general user experiments to perform mainly high-resolution (Fig. 3) and in-situ studies, respectively.
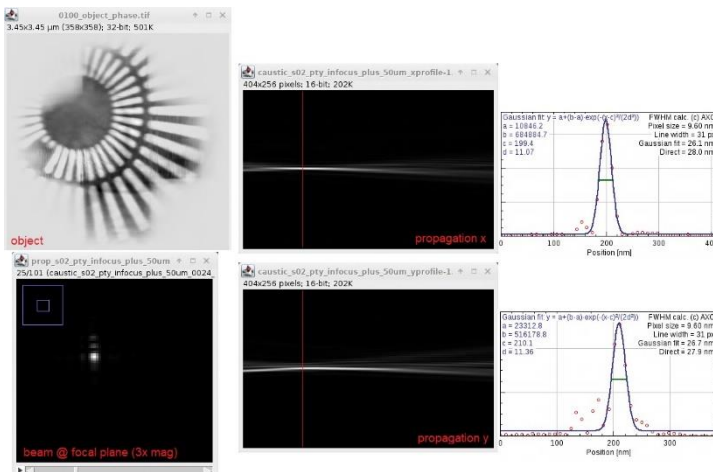

Fig.3: Results of the ptychographic reconstruction of sample (Siemens star) and illumination beam of the high-resolution MLL setup; The propagation of the reconstructed beam shows a non-astigmatic caustic with a focal spot of approx. **28x28 nm² size** (beamtime 2021/I).

- The in-situ indenter, whose development started already during the previous LTP, was further optimized and in September 2021 finally handed over to ESRF (Fig. 4). For this purpose, Dr. Juraj Todt spent ~two weeks at ID13 and helped to implement the hardware and the software (directly into BLISS).
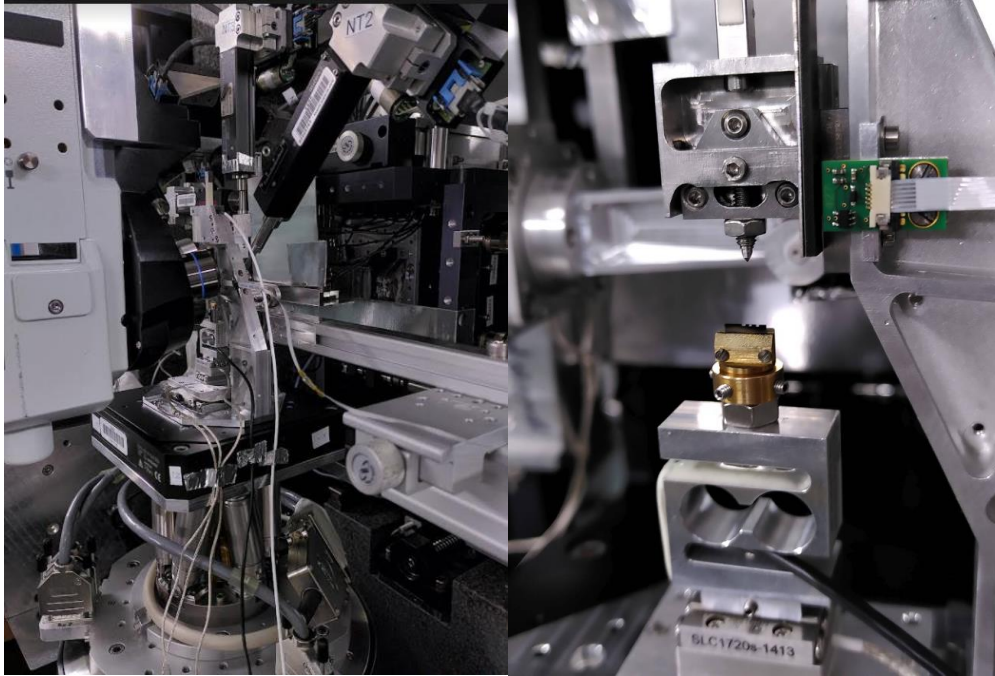

Fig. 4: Indentation system designed by the Leoben group and handed over to ESRF in September 2021 (beamtime 2021/II).

- The first *in situ* SAXS and WAXS studies coupled with a sample loading were performed using the new indenter at ID13 (Fig. 5) and the long-distance MLLs optins. The data were recorded in a mesh of $x \times y$ = 30×36 µm² using a step of 60 nm in both x and y directions leading to 300,000 2D diffractograms for each load step during indentation. Fig. 5a shows a SEM image of the deformed cantilever. The X-ray data presented in Fig. 5b-d shows the cantilever's state after deformation. The SAXS-data (Fig. 5b) give unprecedented insight into shear-band formation and propagation during loading, while FWHM data (Fig. 5c) show defect accumulation in front of the crack tip and the plastically deformed area at the lower end of the cantilever. Fig. 5d shows the residual axial stresses in the deformed cantilever and gives insight into crack closing and stress build up after unloading.
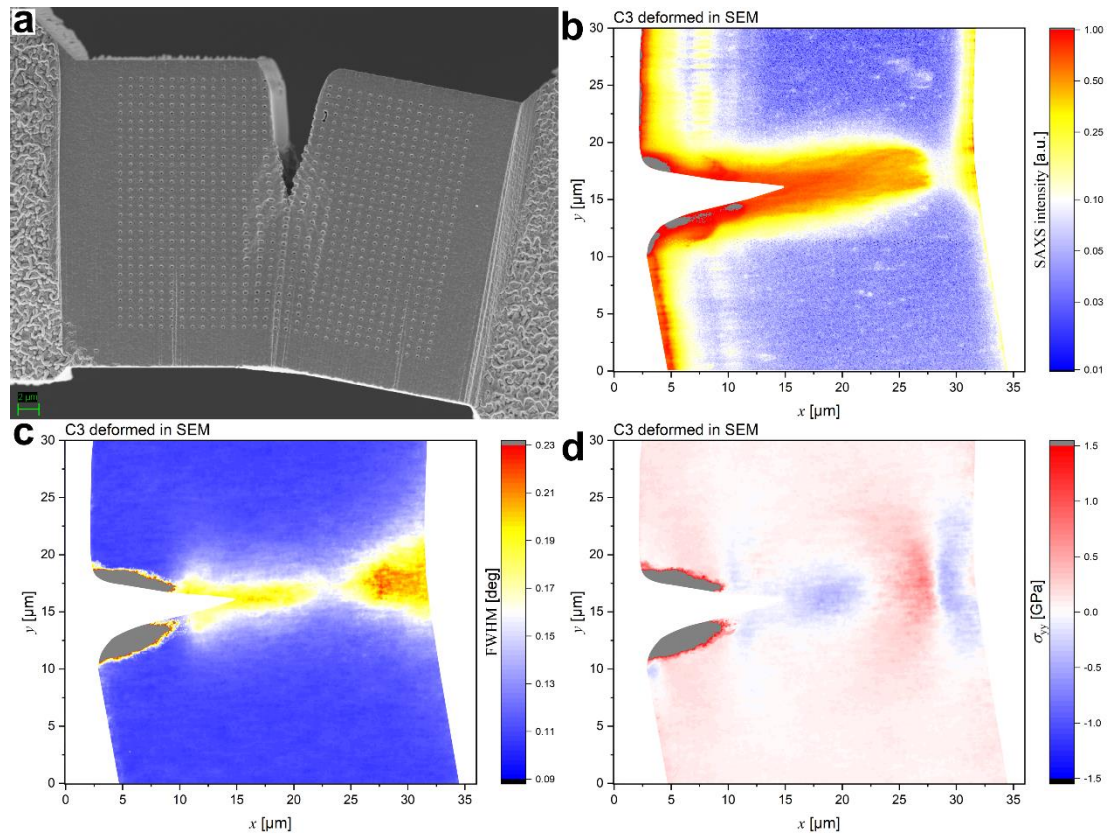
Fig. 5: Results from an in-situ loaded micro-cantilever using a new indentation system and new long-distance MLLs at ID13. The cantilever imaged in SEM after loading is shown in (a), SAXS intensity from the sample is presented in (b), averaged FWHM distributions representing defect build-up is given in (c) and the axial stresses showing the compressive stress accumulation in front of the closed crack is shown in (d). (beamtime 2021/II).

Year 2

A prototype of a new housing with an integrated motorized adjustment for the most critical degree of freedom of the relative alignment of both lamellae – the perpendicularity – and few other improvements was tested. This device supersedes the dedicated alignment fixture, which is currently used to perform the internal lens alignment. It allows an intermediate correction for aberrations by the beamline staff, if required, what makes the MLLs more reliable for user experiments. Ready-adjusted MLL optics were always left for several users' experiments at the beamline after the individual beamtimes of the LTP. This approach will be continued to gain further experience with the use of our optics for general scientific cases and to improve the capabilities of ID13.

Figs. 6 and 7 show some of the results using a photon energy of 13 keV. Two designs were tested: The "high resolution" design (Fig. 6) aims for small spots with sub-25 nm FWHM at moderate working distances of ≥ 3 mm behind the required order-sorting aperture. Improvements in the preparation of the lenses and the new housing resulted in a minimization of the astigmatism. A combined efficiency of $\eta^2 = 29 \%$ was measured for an effective geometrical aperture of ≈ 40 µm × 45 µm. The "long working distance" design (Fig. 7) aims for sub-100 nm spots, larger geometrical apertures and > 20 mm clearance to allow complex experimental setups around the focal spot. A combined efficiency of $\eta^2 ≈ 60 \%$ was measured for an effective geometrical aperture of ≈ 75 µm × 75 µm.
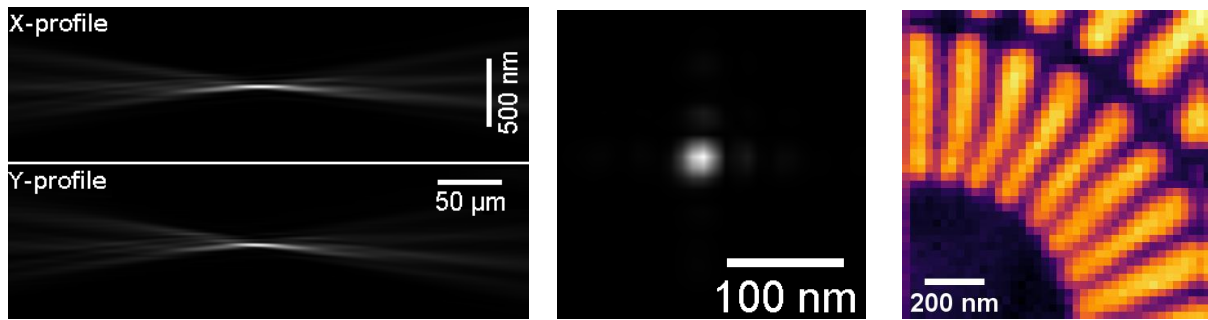
Figure 6: Horizontal and vertical caustic of the "high-resolution" MLL showing no astigmatism; reconstructed intensity in the focal plane indicating a 23 nm FWHM focus with minor sidelobes; and map with the recorded transmitted intensity of a central raster scan of a 1 μm × 1 μm area of the Siemens star test pattern showing a good contrast and no evidence for any critical aberrations for the "high resolution" design.
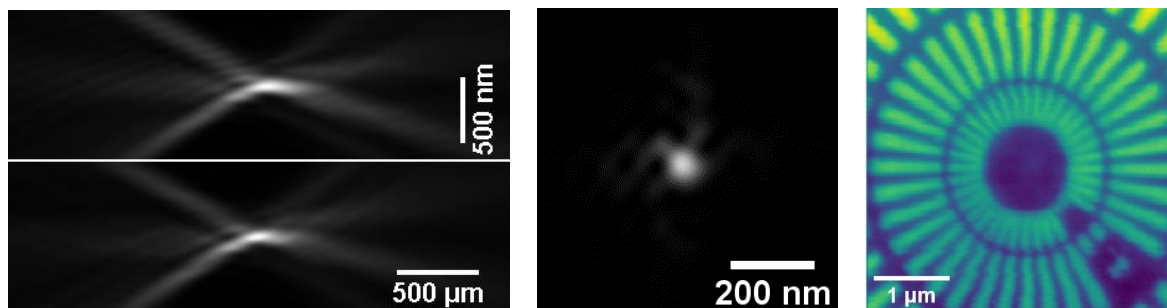

Figure 7: Horizontal and vertical caustic of the "long working distance" MLL showing no astigmatism; reconstructed intensity in the focal plane indicating a 90 nm FWHM focus with minor sidelobes; and map with the recorded transmitted intensity of a central raster scan of a 4 μm × 4 μm area of the Siemens star test pattern with good contrast.

During the January 2022 experiment, several tests using the indenter system were performed. Using the indenter setup transferred to ID13, a new possibility to measure the X-ray elastic strain (henceforth transformed to stress) and the total strain independent from each other within one experiment was used for the first time.

In order to perform this experiment, cantilevers from nanocrystalline super-saturated FeCr were fabricated using focused ion beam (FIB) milling (*cf*. Fig. 8). After final polishing of the cantilevers the gas injection system (GIS) of the FIB was used to deposit platinum dots on the cantilevers surface in order to trigger a strong SAXS signal (Fig. 8b,c). The displacement of the individual Pt dots during the synchrotron experiment is tracked using the SAXS microscopy introduced by the Leoben group during the last LTP.
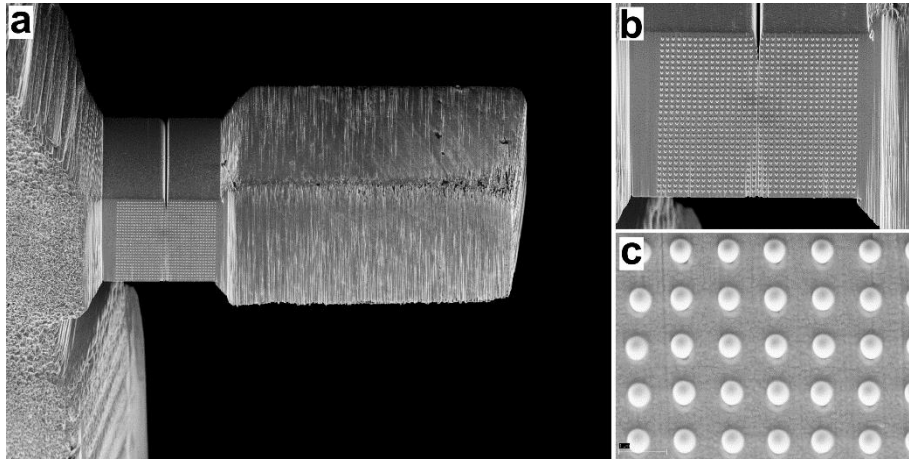
Fig. 8: (a) A SEM image of a finished cantilever tested in 01/2022 at ID13 beamline at ESRF. (b) The region of interest showing the platinum dots deposited using the built-in gas injection system of the FIB and (c) an high-resolution SEM image of the platinum dots (c).

The experiment showed, that the Pt dots are amorphous and form clusters with a distinctive size distribution (*cf*. Fig. 9). A micrograph compiled using the integrated signal around the beam stop, which is primarily sensitive to the local electron density variations originating in the Pt dots is presented in Fig. 10b.
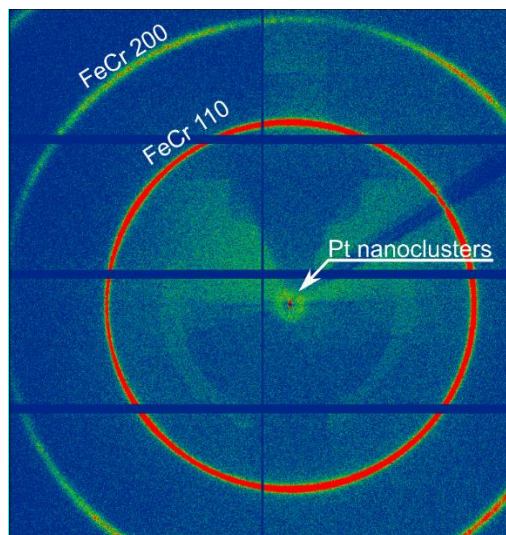

Fig. 9: A detector image showing the WAXS 110 and 200 rings of the nanocrystalline FeCr as well as the SAXS signal originating from the nanoclustered Pt dots

The cantilever containing the Pt dot pattern on the surface in the region of interest was loaded step-wise (*cf*. Fig. 10a) and 11 2D maps containing ~250,000 2D diffractograms were recorded using a step size of 60 nm. A comparison with an experiment on a similar cantilever deformed in the SEM showed that the load-displacement curves and thus the deformation behaviour are similar.
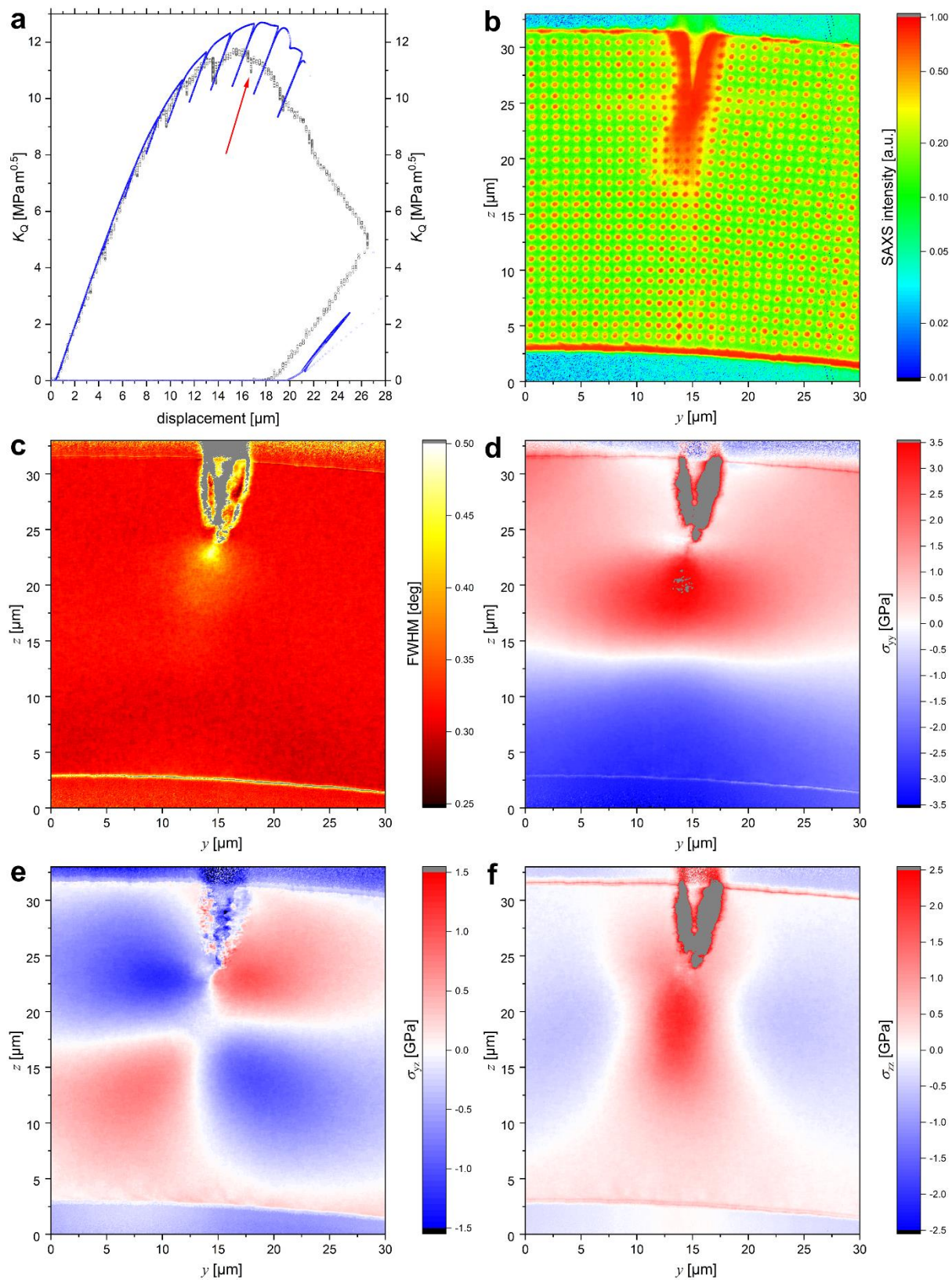
Fig. 10: Data recorded from an elastic-plastic nanocrystalline supersaturated solid solution FeCr. In (a), the applied K_Q-displacement curves are shown for a cantilever deformed in SEM (blue) and at the ESRF (dotted), confirming good agreement with continuous testing in SEM. In (b), the integrated signal from the Pt dots is pesented, which is used for measuring total strain. In (c) an averaged FWHM map is shown, giving insight into the local intracrystalline defect density, while in (d-f), the σ_{yy}, σ_{yz} and σ_{zz} stress distributions are presented, respectively.

Furthermore, the FWHM distribution gives insight into the regions were intracrystalline defects are formed as a consequence of the loading segments and the associated stress distributions are presented in Fig. 10d-f. The unique combination of stress and strain measurement within one sample allows to determine locally the total energy dissipated by the deformation of the material and furthermore allows to directly assess the local J, which is the parameter defining elastic-plastic crack growth. Both parameters are not usually directly accessible by other (micro-)mechanical experiments.

In addition, scanning experiments on thin films, coatings and MOSFET transistors were performed. In Fig. 11, an exemplary scan from transistor is shown. Selected results were published in August 2022 in [https://doi.org/10.1016/j.mtla.2022.101484] and the results will appear also in the ESRF Highlights 2022, in the chapter Industrial Research.
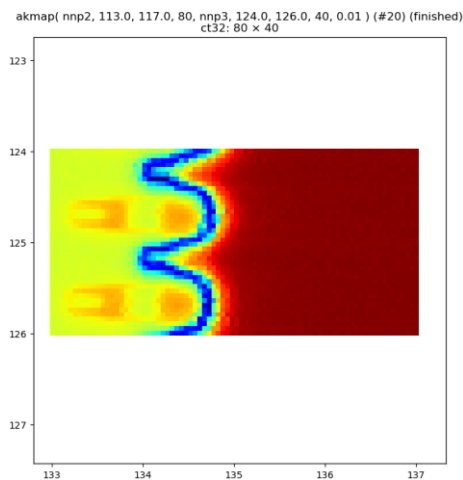

Fig. 11: An absorption scan indicates the distribution of features at the cross-section of the MOSFET transistor. The results were published in [https://doi.org/10.1016/j.mtla.2022.101484]. **The results are expected to be featured in ESRF Highlight 2022.**

During the May 2022 experiment, a new operando setup was tested for the first time. The aim was to track Li dendrite growth through a LLZO-based Li-ion battery solid-state electrolyte (Fig. 12). The results from the measurements (Fig. 12) were submitted for publication in Nature Communications.

Fig. 12: A new setup to cycle solid state battery was tested at the ID13 (beamtime May 2022/II).
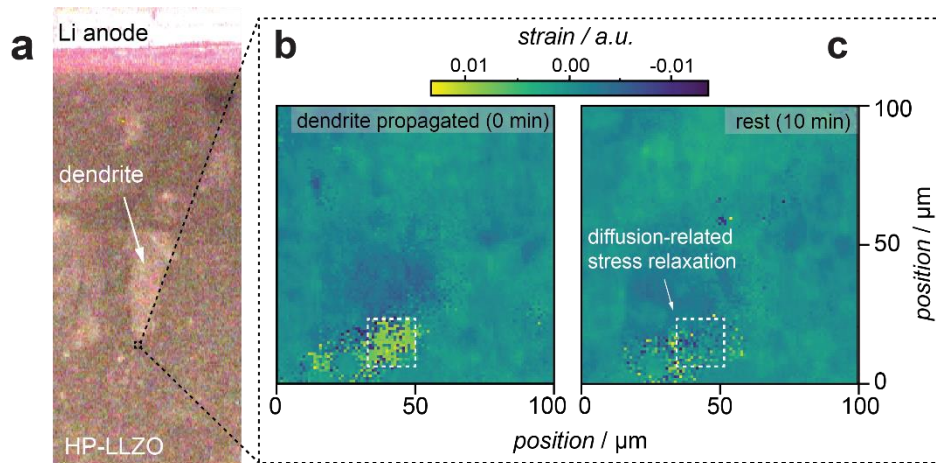
Fig. 13. Mechanism and operando CSnanoXRD characterization. (a) The dendrite is highlighted in an optical microscope overview image, while the mapped region of 10 × 10 μm is marked as a black-dashed square. The LLZO-HP material is polycrystalline. Corresponding operando synchrotron X-ray nano diffraction strain maps show a region directly ahead of a Li dendrite directly after its growth and after a waiting time of approx. 10 min. A single grain is highlighted and exhibits a deviatoric strain of approx. 0.0045 (b), while it has relaxed to -0.0015 (c), equivalent to a change in deviatoric stress of approx. 750 MPa. This relaxation was not seen when comparing the state (i) during the dendrite's growth and (ii) directly thereafter. The grain is located approx. 8-10 μm in front of the supposed location of the Li dendrite's tip.

Year 3

4. List of publications directly resulting from beamtime used for this Long Term Project:

- Jäger, N., Meindlhumer, M., Zitek, M., Spor, S., Hruby, H., Nahif, F., Julin, J., Rosenthal, M., Keckes, J., Mitterer, C., Daniel, R. Impact of Si on the high-temperature oxidation of AlCr(Si)N coatings (2022) Journal of Materials Science and Technology, 100, pp. 91-100. DOI: https://doi.org/10.1016/j.jmst.2021.04.065

- Spor, S., Jäger, N., Meindlhumer, M., Hruby, H., Burghammer, M., Nahif, F., Mitterer, C., Keckes, J., Daniel, R. Evolution of structure, residual stress, thermal stability and wear resistance of nanocrystalline multilayered Al0.7Cr0.3N-Al0.67Ti0.33N coatings (2021) Surface and Coatings Technology, 425, art. no. 127712. https://doi.org/10.1016/j.surfcoat.2021.127712

- Hlushko, K., Mackova, A., Zalesak, J., Burghammer, M., Davydok, A., Krywka, C., Daniel, R., Keckes, J., Todt, J. Ion irradiation-induced localized stress relaxation in W thin film revealed by cross-sectional X-ray nanodiffraction (2021) Thin Solid Films, 722, art. no. 138571. https://doi.org/10.1016/j.tsf.2021.138571#

- Michael Meindlhumer, LR Brandt, Jakub Zalesak, M Rosenthal, Hynek Hruby, J Kopecek, E Salvati, Christian Mitterer, Rostislav Daniel, Juraj Todt, Jozef Keckes, Alexander M Korsunsky, Evolution of stress fields during crack growth and arrest in a brittle-ductile CrN-Cr clamped-cantilever analysed

by X-ray nanodiffraction and modelling, Materials & Design 198, 15 January 2021, 109365. https://doi.org/10.1016/j.matdes.2020.109365

- S. Karner, O. Blank, M. Rösch, M. Burghammer, J. Zalesak, J. Keckes and J. Todt, X-ray nanodiffraction analysis of residual stresses in polysilicon electrodes of vertical power transistors, Materialia 24 (2022) 101484. https://doi.org/10.1016/j.mtla.2022.101484
  The results are expected to be featured in ESRF Highlight 2022.

- Frank, F., Tkadletz, M., Saringer, C., Czettl, C., Pohler, M., Burghammer, M., Todt, J., Zalesak, J., Keckes, J., Schalk, N. ; Investigation of the microstructure of a graded ZrN/Ti0.33Al0.67N multilayer coating using cross-sectional characterization methods (2023) Surface and Coatings Technology, 453, art. no. 129126, DOI: https://doi.org/10.1016/j.surfcoat.2022.129126

- Meindlhumer, M., Ziegelwanger, T., Zalesak, J., Hans, M., Löfler, L., Spor, S., Jäger, N., Stark, A., Hruby, H., Daniel, R., Holec, D., Schneider, J.M., Mitterer, C., Keckes, J. Precipitation-based grain boundary design alters Inter- to Trans-granular Fracture in AlCrN Thin Films (2022) Acta Materialia, 237, art. no. 118156. https://doi.org/10.1016/j.actamat.2022.118156

- Rostislav Daniel, Jakub Zalesak, Igor Matko, Walter Baumegger, Anton Hohenwarter, Easo P George, Jozef Keckes, Microstructure-dependent phase stability and precipitation kinetics in equiatomic CrMnFeCoNi high-entropy alloy: Role of grain boundaries, Acta Materialia 223 (2022) 117470, https://doi.org/10.1016/j.actamat.2021.117470